The Lysosomal Potassium Channel TMEM175 Adopts a Novel Tetrameric Architecture

Changkeun Lee[1,2], **Jiangtao Guo**[1], **Weizhong Zeng**[1,2], **Sunghoon Kim**[1,2], **Ji She**[1], **Chunlei Cang**[3], **Dejian Ren**[3], and **Youxing Jiang**[1,2]

[1]Department of Physiology and Biophysics, University of Texas Southwestern Medical Center, Dallas, Texas 75390-9040

[2]Howard Hughes Medical Institute, University of Pennsylvania, Philadelphia, Pennsylvania 19104

[3]Department of Biology, University of Pennsylvania, Philadelphia, Pennsylvania 19104

Abstract

TMEM175 is a lysosomal K^+ channel important for maintaining the lysosomal membrane potential and pH stability[1]. It contains two homologous copies of a six-transmembrane (6-TM) domain, which has no sequence homology to the canonical tetrameric K^+ channels and lacks the TVGYG selectivity filter motif[2–4]. Present in a subset of bacteria and archaea, the prokaryotic TMEM175 contains only a single 6-TM domain and functions as a tetramer. Here, we present the crystal structure of a prokaryotic TMEM175 from *Chamaesiphon minutus*, CmTMEM175, whose architecture represents a completely different fold from that of canonical K^+ channels. All six transmembrane helices of CmTMEM175 are tightly packed within each subunit without undergoing domain swap. The highly conserved TM1 acts as the pore lining inner helix, creating an hour-glass shaped ion permeation pathway in the channel tetramer. Three layers of hydrophobic residues on the C-terminal half of TM1s form a bottle neck along the ion conduction pathway and serve as the selectivity filter of the channel. Mutagenesis analysis suggests that the first layer of the highly conserved isoleucine residues in the filter plays the central role in channel selectivity. Thus, the structure of CmTMEM175 represents a novel architecture of a tetrameric cation channel whose ion selectivity mechanism appears distinct from that of the classical K^+ channel family.

Acidic lysosomal organelles mediate crucial biological processes such as degradation, catabolite export, and metabolism-sensing[5–7], and defects to these processes can result in lysosomal storage diseases[8–10]. The lysosomal membrane is decorated with channels and transporters that regulate the lysosome's ionic homeostasis and physiological functions[5,11,12]. Recently, a previously uncharacterized transmembrane protein 175

*Address correspondence to: Youxing Jiang, Ph.D., Department of Physiology, UT Southwestern Medical Center, 5323 Harry Hines Blvd., Dallas, Texas 75390-9040, Tel. 214 645-6027; Fax. 214 645-6042; youxing.jiang@utsouthwestern.edu.

The authors declare no competing financial interests.

(TMEM175) was identified as the *bona fide* endo/lysosomal K^+ channel, whose function is important for setting the lysosomal membrane potential and maintaining pH stability[1]. TMEM175 deficiency has been shown to play a critical role in Parkinson disease pathogenesis[13,14].

The mammalian TMEM175 contains two homologous 6-TM domains and is suggested to function as a dimer[1]. Since TMEM175 lacks the TVGYG motif and sequence homology to canonical 6-TM K^+ channels[2–4], it is predicted to adopt a distinct structure and K^+ selectivity mechanism from classical K^+ channels. Present among some bacteria and archaea, the prokaryotic TMEM175 (bacTMEM175) contains a single copy of a 6-TM domain in each subunit (Extended Data Fig. 1). Several bacTMEM175s can be overexpressed and purified as tetramers in solution (Extended Data Fig. 2), supporting the prediction that eukaryotic TMEM175 with two 6-TM domains functions as a dimer. The bacTMEM175 from *Chamaesiphon minutus*, CmTMEM175, yielded the best diffracting crystals and will be the focus of this study.

We first tested if CmTMEM175 functions as a K^+-selective channel. Unable to record CmTMEM175 channel current using electrophysiology, we therefore utilized a ^{86}Rb flux assay[15] to measure K^+ permeation and selectivity, based on the premise that CmTMEM175 can conduct K^+ as well as Rb^+ (Methods). Briefly, CmTMEM175 was reconstituted into liposomes containing high concentrations of KCl. Upon exchanging the proteoliposomes to a low salt reaction buffer containing ^{86}Rb, the K^+ concentration gradient across the liposomal membrane drives K^+ efflux through CmTMEM175, generating an electrical driving force for the influx of radioactive ^{86}Rb (Methods). Fig. 1a shows the time-dependent accumulation of ^{86}Rb inside K^+-loaded proteoliposomes, confirming that CmTMEM175 is permeable to K^+ and Rb^+. The same flux assay performed using proteoliposomes loaded with NaCl shows much weaker liposomal ^{86}Rb accumulation (Fig. 1b), indicating that CmTMEM175 conducts K^+ better than Na^+.

To evaluate channel selectivity, we performed a competition assay by measuring ^{86}Rb influx in the presence of various external monovalent cations; conductive ions would compete with ^{86}Rb and decrease its liposomal accumulation over time. The competition assay indicates that CmTMEM175 is permeable to K^+, Rb^+ and Cs^+, which caused a reduction in ^{86}Rb accumulation in comparison to the control experiment (Fig. 1c). The channel is unable to conduct Na^+ and the large organic cation N-methyl-D-glucamine ($NMDG^+$), both of which have no obvious effect on ^{86}Rb influx. These results show that CmTMEM175 is selective for K^+, Rb^+ and Cs^+ over Na^+, consistent with the selectivity of the eukaryotic TMEM175.

The structure of CmTMEM175 was determined and refined to 3.3 Å (Methods and Extended Data Fig. 3). Consistent with biochemical data, CmTMEM175 adopts a 4-fold symmetric, square-shaped tetramer in the crystal with a dimension of about 61 Å on each side and a height of about 60 Å (Fig. 2). Each subunit contains six transmembrane (TM) helices with both N- and C- termini predicted to be on the cytosolic side. TMs 1-3 are positioned on the inner circle of the channel tetramer and participate in inter-subunit interactions central to the assembly of the ion conduction pore. TMs 4-6 are positioned on the periphery of the channel and do not contribute to any contacts with neighboring subunits. Not surprisingly, TMs 1-3

have higher sequence conservation than TMs 4-6 among TMEM175 homologs. TM1 and 2 are linked by an extended, strand-like tail and two short helices (H1 and H2). This linker protrudes outward from the main body of the transmembrane domain and encloses the external open entrance of the ion conduction pore in the channel tetramer. TM3 is bent into two segments (TM3a and TM3b) due to the presence of a conserved proline (Pro102) (Fig. 2 and Extended Data Fig. 1).

In comparison, the structure of CmTMEM175 is completely different from that of canonical 6-TM homo-tetrameric K$^+$ channels[16,17] (Extended Data Fig. 4). First, all six transmembrane helices of CmTMEM175 are tightly packed within each subunit without undergoing any domain swap. Second, the two central pore elements in canonical K$^+$ channels, the pore helix and the TVGYG selectivity filter, are not present in CmTMEM175. Third, in CmTMEM175, TM1 instead of TM6 forms the pore-lining inner helix at the center of the channel. Finally, a search of the structure database using DALI[18] yields no similar structures, indicating that the 6-TM architecture of CmTMEM175 represents a new fold.

The pore-lining TM1 represents the most conserved region in the TMEM175 family. Four TM1 helices form a bundle crossing, which, along with their extended C-terminal tails, create an hour-glass shaped ion permeation pathway (Fig. 3a-c). No specifically bound ions were observed along the pathway even in crystals soaked with heavier mono- or divalent cations. The bundle crossing juncture contains three layers of highly conserved hydrophobic residues – Ile23s, Leu27s and Leu30s – that form a 10-Å long bottle neck with a diameter of about 3 Å at each constriction point. The N-terminal half of TM1 lines the cytosolic entrance of the hour-glass pathway with a negatively charged surface potential (Fig. 3d) while the extended C-terminal tail of TM1 along with the C-terminal half of TM3 (TM3b) enclose the extracellular entrance of the pathway with a slightly negative surface potential.

The N-terminal part of TM1 also contains the $_{12}$RxxxFSD$_{18}$ signature sequence motif that is important for TMEM175 channel function[1]. These residues coordinate a network of specific inter- and intra-subunit interactions with several other highly conserved residues on TM2 and 3 and play a crucial role in the tetrameric assembly of the channel. As shown in Fig. 3e, Arg12 forms cation-π interaction with His74 from TM2 of a neighboring subunit; Phe16 forms π-π stacking with Trp70 from TM2 of the neighboring subunit; Ser17 forms an intra-subunit H-bonding network with His73 on TM2 and Asn91 on TM3; Asp18 forms a hydrogen bond with Trp70 of same subunit, which participates in the π-π stacking with Phe16 of the neighboring subunit.

With wide open entrances on both sides of the membrane, the only possible region that can control ion flux of CmTMEM175 is the narrow hydrophobic bottle neck. Intuitively, this poses a conundrum given our understanding of what constitutes a K$^+$ selective ion conduction pore: How can charged ions move across this narrow tunnel whose size is equivalent to a closed tetrameric cation channel gate[19,20,21]? However, ion permeation through a narrow hydrophobic pathway is not unprecedented. One example is the pentameric bestrophin channel in which three layers of hydrophobic residues create a 10Å long, 3Å wide ion pathway resembling that of CmTMEM175 (Extended Data Fig. 5)[22,23]. Intriguingly, the animal Bestrophin channel, whose narrow pathway is formed by three

layers of Ile, Phe, and Phe, is an anion selective channel while the bacterial Bestrophin, which contains Ile, Ile, and Phe at the bottle neck, has been shown to be cation selective channel[22,24,25].

To examine the potential role of the narrow hydrophobic bottle neck of TMEM175 in controlling ion selectivity, we performed a series of mutagenesis on the three layers of hydrophobic residues (Extended Data Fig. 6a) in human TMEM175 (hTMEM175) expressed in HEK293 cells. The plasma membrane-localized hTMEM175 channel activity can be measured using whole-cell patch clamping (Methods), which exhibits the same K^+ and Cs^+ selectivity as well as the pharmacological properties (i.e. Zn^{2+} and 4-AP blockage) as previously observed by the lysosomal patch method[1] (Extended Data Fig. 6). When the 2nd or the 3rd layer of hydrophobic residues were replaced by alanine, either individually or collectively, the mutant channels remain K^+/Cs^+ selective (Fig. 4a and Extended Data Fig. 6g). However, the first layer Ile residues are highly sensitive to mutations and no channel activity was observed when they were mutated to Val, Leu, Phe or Ala. Interestingly, the two Ile residues can be replaced with Asn, resulting in a mutant channel that is no longer K^+/Cs^+ selective (Fig. 4a and Extended Data Fig. 6e-h). These results suggest that the Ile residues at the internal mouth of the narrow pathway play the central role in selectivity.

We also performed mutagenesis on the first layer of Ile residues (Ile23s) on CmTMEM175 by replacing them with Cys, Ala, or Asn, and analyzed the selectivity using the ^{86}Rb flux assay. These mutants were expressed, purified and reconstituted into the liposomes loaded with KCl, and their selectivity was measured by a competition assay with external K^+, Na^+ or $NMDG^+$ (Fig. 4b). Both external K^+ and Na^+, but not $NMDG^+$, resulted in a concentration-dependent decrease of ^{86}Rb influx into proteoliposomes of the CmTMEM175 mutants, indicating that the mutant channels can conduct both Na^+ and K^+. This result confirms the central role of the layer 1 Ile23 in defining the K^+ selectivity of CmTMEM175.

With a structure so different from canonical K^+ channels, how does TMEM175 achieve its K^+ selectivity? The narrow hydrophobic filter of CmTMEM175 is reminiscent of hydrophobic nanochannels such as synthetic organic nanopore or single-walled carbon nanotube and the radius-dependent selectivity of these nanochannels might provide a plausible explanation[26–29]. Computationally, nanochannels with a sub-nanometer pore size (i.e. r < 5 Å) have been suggested to achieve higher selectivity for K^+ over Na^+, because the energetic cost of shedding water from the ion hydration shell or constraining a hydrated ion inside a narrow hydrophobic pore is lower for K^+ than Na^+. With an extremely narrow hydrophobic pathway of 3 Å in diameter, ion passage through the TMEM175 filter has to be in a partially dehydrated form with only two coaxial water molecules remaining, one on each side, and is expected to be energetically unfavorable. Two features of the TMEM175 structure may help in overcoming the energy barrier for ion passage. First, the electronegative surface potential on both entrances can attract and stabilize the positively charged ions and effectively increase the local cation concentration. Second, the hour glass architecture of the ion pathway effectively reduces the thickness of the membrane barrier, allowing for the membrane potential to drop across the 10 Å filter region and, thereby, significantly enhances the electrochemical driving force for ion permeation. It is also worth noting that the narrow pathway observed in the CmTMEM175 structure likely represents a closed filter with the

minimum size as the side chain of two neighboring Ile23s is only about 3.3 Å apart (Fig. 3), reaching the closest van der Waals distance between two non-covalent carbon atoms. It is unclear how TMEM175 is gated, but we suspect that the filter also serves as the channel gate whose size could be wider than 3 Å upon opening. In conclusion, our structural and functional studies on CmTMEM175 offer an unconventional way of looking at a presumed complete story on the selectivity of the well-studied family of tetrameric K^+ channels.

Methods

Protein expression and purification

20 genes of prokaryotic TMEM175 homologs were chemically synthesized (Biomatik), sub-cloned into pET15b expression vectors and tested for expression in *E. coli*. Several of them can be over-expressed in *E.coli*, stabilized in *n*-decyl-ß-D-maltopyranoside (DM) detergent, and purified to homogeneity. TMEM175 from *Chamaesiphon minutus* (CmTMEM175) yields the best diffracting crystals for structure determination in this study and will be used for the description of protein expression and purification. The full-length *Chamaesiphon minutus* TMEM175 (NCBI: WP_015160509.1) gene was sub-cloned into pET15b vector (Novagen) with the resulting construct containing sequences for an N-terminal hexahistidine tag and thrombin cleavage site. *E. coli* BL21 (DE3) cells were transformed, cultured in 2YT medium initially at 37 °C to the optical density (OD_{600}) of 0.4, and then at a reduced temperature of 30 °C; overexpression was induced with 0.1 mM isopropyl β-D-thiogalactoside (IPTG) at the OD_{600} of 0.6. Cells were harvested 6 hours after induction and homogenized with an emulsiflex-C5 homogenizer (Avestin) in buffer containing 50 mM HEPES, pH 7.4, 200 mM KCl, 1 μg/mL leupeptin, 1 μg/mL pepstatin A, 2 μg/mL DNaseI, 1 μg/mL Aprotinin, and 1 mM PMSF. Cell lysate was incubated with 1% (w/v) *n*-dodecyl-β-D-maltopyranoside (DDM; Anatrace) for 3 hours at room temperature for protein extraction. The supernatant was collected after a 45-minute centrifugation at 48,384 g, supplemented with 5 mM imidazole and loaded onto a Talon Co^{2+} affinity column (Clontech) pre-equilibrated with 20 mM HEPES pH7.4, 200 mM KCl, and 1 mM DDM. The protein was eluted with the equilibration solution containing 300 mM imidazole and digested overnight at 4 °C with Thrombin (1 Unit/5g wet cells; Roche) to remove the hexahistidine tag. The sample after digestion was concentrated using 100 KDa cut-off Amicon Centrifugal Filter (EMD Millipore) and further purified by gel filtration using a Superdex-200 (10/30 GL) column (GE Healthcare) in 20 mM HEPES, pH 7.4, 200 mM KCl, 0.5 mM decyl maltose neopentyl glycol (DMNG, for crystallization and functional assays) or 3 mM *n*-decyl-β-D-maltopyranoside (DM, for biochemical assays). Peak fractions were collected and concentrated for further experiments. To facilitate model building, more than ten CmTMEM175 mutants with a single-cysteine substitution at various parts of the protein were generated using QuikChange II Site-Directed Mutagenesis Method (Agilent). All mutants were expressed, purified and crystallized in similar conditions as the wild-type protein.

Crystallization

CmTMEM175 was purified in DMNG and concentrated to 6 mg/mL for crystallization. Crystals were grown at 20 °C using sitting-drop vapor diffusion method. Crystals appeared

within 3 days in a condition of 16-22% PEG 1000, 50 mM $CaCl_2$, 50 mM $MgCl_2$ and 100 mM NaAc, pH 4.6, and grew to their full size in 2-4 weeks. Crystals were cryo-protected by adding the cryo-solution containing 25% PEG 1000, 10% glycerol, 50 mM $CaCl_2$, 50 mM $MgCl_2$, 0.5 mM DMNG and 100 mM NaAc, pH 4.6 directly into the crystallization drop and flash-frozen in liquid nitrogen. To obtain experimental phasing, crystals were derivatized overnight by adding methyl mercury chloride (CH_3HgCl) solubilized in the stabilization solution of 25% PEG 1000, 50 mM $CaCl_2$, 50 mM $MgCl_2$, 0.5 mM DMNG, 100 mM NaAc, pH 4.6 into the crystallization drops to a final concentration of 1 mM.

Two different types of crystals were obtained under the same crystallization conditions, one has a $C2$ space group and the other is $P1$. $C2$ crystals diffracted up to 3.3 Å and were used for structure determination, whereas $P1$ crystals generally diffracted up to 4.0 Å. We noticed that freshly purified protein tended to be crystallized in $P1$ space group, whereas leaving purified protein on ice for three days before crystallization yielded more $C2$ crystals. The structures of $P1$ crystals were also determined by molecular replacement method using wild type $C2$ crystal structure as the search model and showed no obvious difference.

Data collection and structure determination

X-ray diffraction data was collected using synchrotron radiation source (Advanced Photon Source 23IDB and 23IDD; Advanced Light Source BL8.2.1 and BL8.2.2). The best diffracting crystal belongs to space group $C2$ with cell dimensions of $a = 152.66$ Å, $b = 108.88$ Å, $c = 119.31$ Å, $a = 90°$, $\beta = 117.24°$, $\gamma = 90°$, and contains four subunits per asymmetric unit. To maximize the anomalous signal, the mercury-derivative data were collected near the mercury absorption edge ($\lambda = 1.0064$ Å).

All diffraction data were integrated and scaled using the HKL2000 package[30]. Since the diffraction data were slightly anisotropic, ellipsoidal truncation, anisotropic scaling and B-factor sharpening were applied to the data using two approaches. For initial phasing and map calculation, "auto-correction" function in HKL2000 was applied to the native and mercury-derivative data, which yielded better experimental maps. For structure refinement, the native data were truncated to 1/3.7 Å^{-1} along a*, 1/3.6 Å^{-1} along b*, 1/3.3 Å^{-1} along c* using the UCLA anisotropy server[31]. After anisotropic scaling, an isotropic B-factor of -67.64 Å^2 was applied.

The structure was determined by single isomorphous replacement with anomalous scattering (SIRAS) using the native and mercury-derivative data (Extended Data Table 1). The heavy atom positions were determined in SHELXD[32] and refined in AutoSharp[33]. The initial phases were improved by solvent flattening with SOLOMON[34], and four-fold non-crystallographic symmetry averaging with RESOLVE[35], generating electron density map of sufficient quality for model building. The model was manually built in COOT[36] and refined with Phenix[37]. To facilitate accurate model building, more than ten mutants containing single cysteine substitution at various parts of the protein were generated, crystallized and derivatized with CH_3HgCl. The heavy atom sites from these mutants as well as wild-type crystals provided unambiguous registry for 11 residues throughout the protein, allowing us to accurately model the structured regions of CmTMEM175. The final model was refined to 3.3 Å with R_{work}=25.9% and R_{free}= 28.2% and contained residues 7-144 and 154-202 from

the protein, covering 93% of the protein sequence. The geometry analysis of the final model with Procheck[38] gave statistics of 97.5% and 2.5% for the most favored and additional allowed regions, respectively, on the Ramachandran plot. The pore radius of the ion conduction pathway was analyzed using the program HOLE[39] and the electrostatic potentials were calculated using the program APBS[40]. All structure figures were prepared with Pymol[41].

Protein reconstitution and ^{86}Rb flux assay

All proteins used in the flux assay were purified in the DMNG detergent and reconstituted into lipid vesicles composed of 1-palmitoyl-2-oleoyl-phosphatidylethanolamine (POPE, 7.5 mg/mL) and 1-palmitoyl-2-oleoyl-phosphatidylglycerol (POPG, 2.5 mg/mL) at a protein/lipid ratio of 2 μg/mg using the same method as described[15] with the following modifications: 20 mM DM was used to solubilize the lipid and the detergent/lipid/protein mixture were dialyzed against a reconstitution buffer of 10 mM HEPES buffered with 4 mM NMDG, pH 7.4, and 450 mM KCl or NaCl to slowly remove the detergent. The reconstituted liposome samples were kept at -80 °C in 100 μL aliquots.

The ^{86}Rb flux assay was performed following the same procedures as described[15]. Liposomes were thawed and sonicated in a bath sonicator for 40 seconds before the assay. To remove extra-liposomal salt (NaCl or KCl), 100 μL samples were passed through a pre-spun Sephadex G-50 fine gel filtration column (1.5 ml bed volume in a 5 ml disposable spin column) swollen in 400 mM Sorbitol, 10 mM HEPES buffered with 4 mM NMDG, pH 7.4. 160 μL of liposome samples collected after this buffer exchange step were added to 320 μL ^{86}Rb flux buffer (400 mM Sorbitol, 10 mM HEPES buffered with 4 mM NMDG, pH 7.4, 50 μM NaCl or KCl, and 5 μM [86]RbCl). At desired time points, 60 μL of this reaction mixture were passed through a pre-spun Sephadex G-50 fine gel filtration column as described above to remove extra-liposomal ^{86}Rb and stop the flux. The eluate was mixed with 10 mL scintillation cocktail and its radioactivity was measured in a scintillation counter. For time dependent measurement of ^{86}Rb influx, the radioactivity of each sample was normalized against the maximum ^{86}Rb influx. The maximum ^{86}Rb influx for K+-loaded liposomes was obtained by adding 1 μg/mL of valinomycin to a 60 μL reaction mixture and allowing the influx to proceed for 2 minutes before sample collection using Sephadex G-50 column. 10 μg/mL of gramicidin A was used to obtain the maximum ^{86}Rb influx for Na+-loaded liposomes. For competition assay, CmTMEM175-containing liposomes were loaded with KCl and flux was allowed to proceed for 30 minutes before the radioactivity levels in liposomes were measured. The tested ions (Na+, K+, Rb+, Cs+ or NMDG+) were added directly into the flux buffer, making the final concentrations of 0.1, 0.5 or 1.0 mM after mixing with liposomes, and samples of reaction mixture were collected 30 minutes after the reaction. The radioactivity of each sample in the competition assay was normalized to the reaction mixture without competition ions.

Chemical cross-linking

Cross-linking experiment were performed using amine-reactive cross-linking reagents disuccinimidyl suberate (DSS) and disuccinimidyl glutarate (DSG, ProteoChem) on bacTMEM175s from *Chryseobacterium sp* and *Streptomyces collinus* following the

manufacturer suggested protocol. Both reagents were prepared as a 50 mM stock in anhydrous dimethylsulfoxide (DMSO). The protein samples used for the cross-linking reactions had a concentration of about 1 mg/mL and were purified in amine-free solution of 20 mM HEPES, pH 7.4, 200 mM KCl and 3 mM DM. The reactions were initiated by adding 2 mM (final concentration) cross-linking reagents to the protein samples and allowed to proceed at room temperature for 5 or 45 minutes. The reactions were quenched by adding Tris, pH 7.4 to a final concentration of 200 mM.

Electrophysiology

Instead of using whole lysosome patch as previously described[1], we were able to express human TMEM175 in HEK293 cells and measure plasma membrane channel activity using whole-cell patch clamping. Human TMEM175 and its mutants were cloned into pCGFP-EU plasmid[42]. 1-2 μg of the plasmid containing the C-terminal GFP-tagged Human TMEM175 or its mutant was transfected into HEK293 cells grown in a six-well tissue culture dish using Lipofectamine 2000 (Life Technology). 24-48 hours after transfection, cells were dissociated by trypsin treatment and kept in complete serum-containing medium and re-plate on 35 mm tissue culture dishes in tissue culture incubator until recording. In most recordings, patch clamp in the whole-cell configuration was employed to measure TMEM175 current in HEK293 cells. Patch clamp in the inside-out configuration was used to measure the Zn^{2+} and 4-AP block of TMEM175 from the intracellular side. The standard extracellular solution contained (in mM): 145 sodium methanesulfonate (Na-MS), 5 NaCl, 1 $MgCl_2$, 1 $CaCl_2$, 10 HEPES buffered with Tris, pH 7.4. The intracellular solution contained (in mM): 150 Cs-MS, 5 $MgCl_2$, 10 EGTA, 10 HEPES buffered with Tris, pH=7.4. The patch pipettes were pulled from Borosilicate glass (Harvard Apparatus) and heat polished to resistance of 3-5 MΩ. Data was acquired using an AxoPatch 200B amplifier (Molecular Devices) and a low-pass analogue filter set to 1 kHz. The current signal was sampled at a rate of 20 kHz using a Digidata 1322A digitizer (Molecular Devices) and further analyzed with pClamp 9 software (Molecular Devices). After the patch pipette attached the cell membrane, the giga seal (5-10 GΩ) was formed by gentle suction. The whole cell configuration was formed by short zap or suction to rupture the patch. The holding potential was set to 0 mV. All I-V curves of TMEM175 and its mutants were obtained using voltage pulses ramp from -100 to +100 mV over 800 ms duration. To measure the ion selectivity, the extracellular solution (bath) was changed to (in mM): 150 XMS (X = Li, K, Rb, or NMDG), 1 $MgCl_2$, 1 $CaCl_2$, 10 HEPES buffered with Tris, pH 7.4. All data points are mean ± SEM (n   5).

The ion permeability ratios were calculated with the following equation:

$$P_{Cs}/P_X = [X]_{ext} / \left([Cs]_{int} exp \left(E_{rev} F/RT \right) \right) (X = Li, \ Na, \ K, \ or \ Rb)$$

where E_{rev} is the reversal potential, F is Faraday's constant, R is the gas constant, and T is the absolute temperature.

Data availability

The atomic coordinates and structure factors have been deposited in the Protein Data Bank under accession number 5VRE.
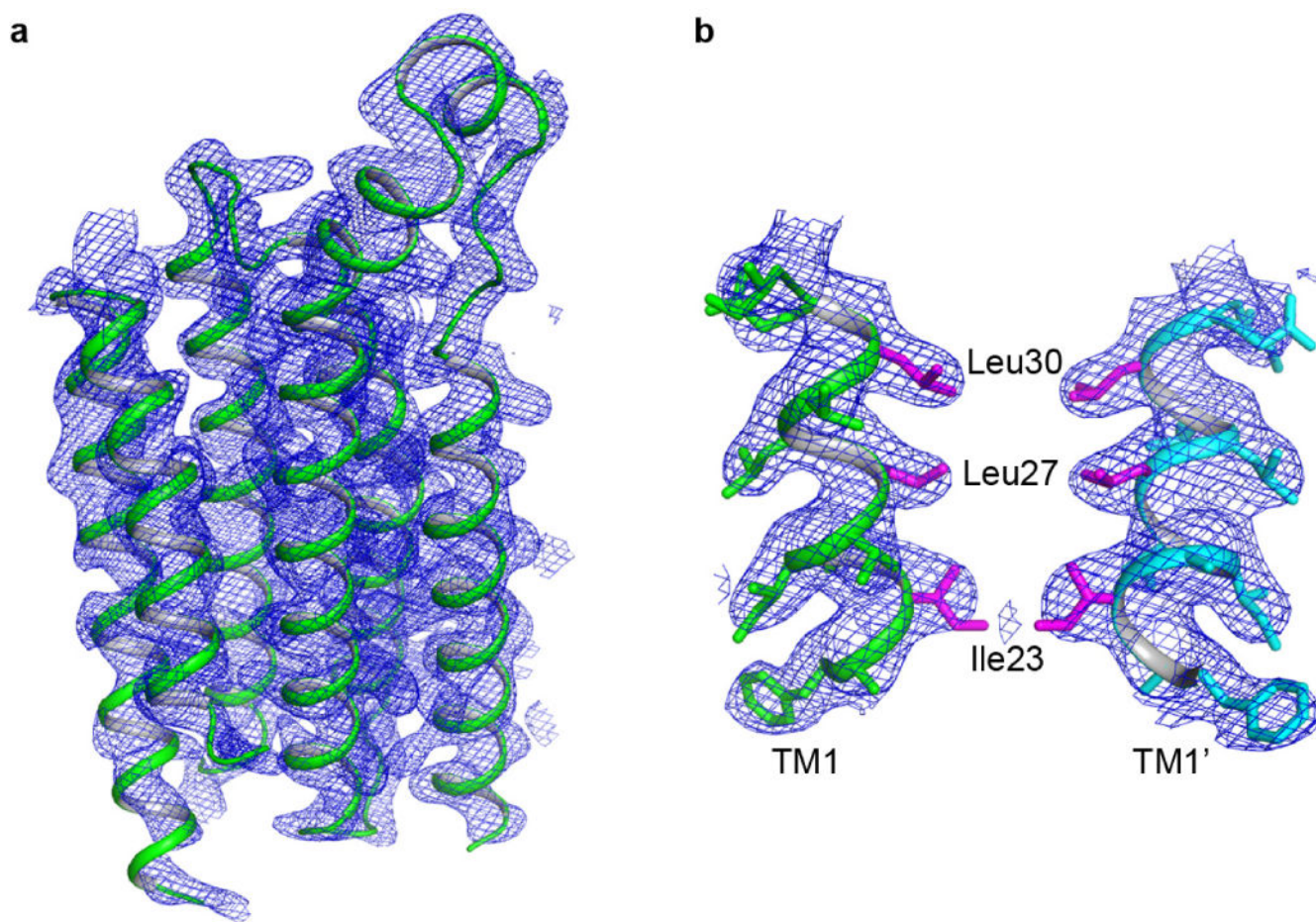
Extended Data

Extended Data Figure 1. Sequence comparison between prokaryotic and eukaryotic TMEM175s

a, Topologies of prokaryotic (left) and eukaryotic (right) TMEM175s. **b**, Sequence alignment of prokaryotic TMEM175s and the first 6-TM domains of eukaryotic TMEM175s. **c**, Sequence alignment of prokaryotic TMEM175s and the second 6-TM domains of eukaryotic TMEM175s. Secondary structure assignments are based on the CmTMEM175 structure. Asterisks mark the three hydrophobic filter residues. Blue triangles mark the RxxxFSD motif and the residues participating in the inter- and intra-subunit interactions with the motif.
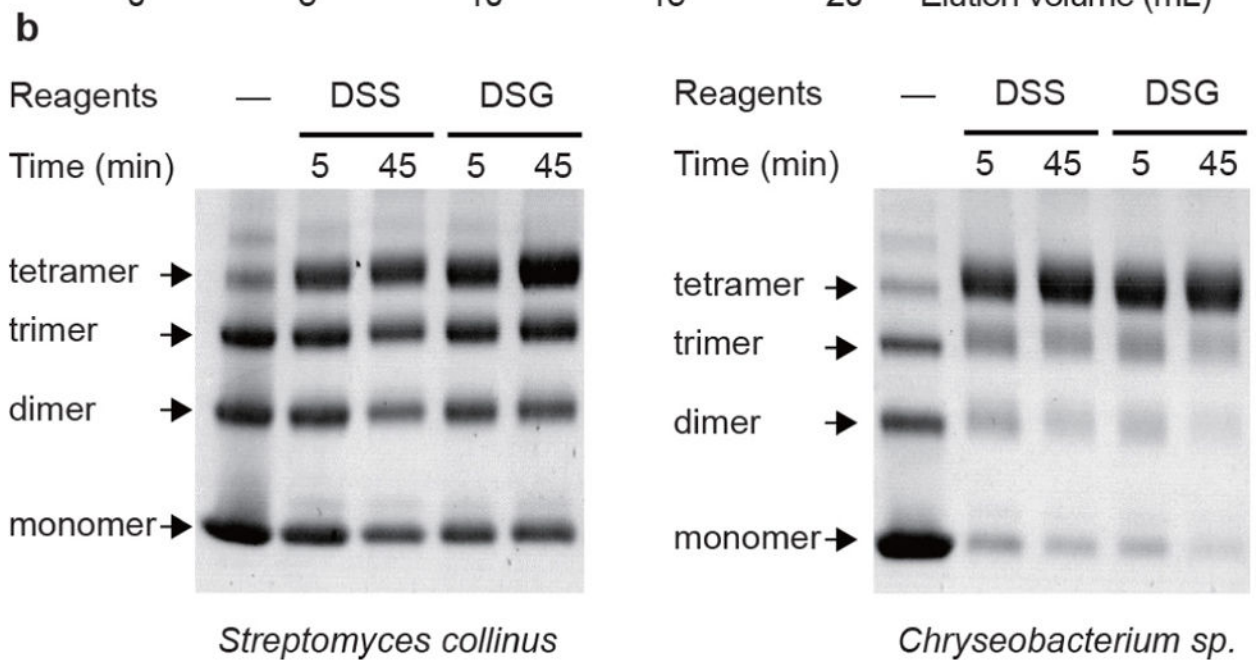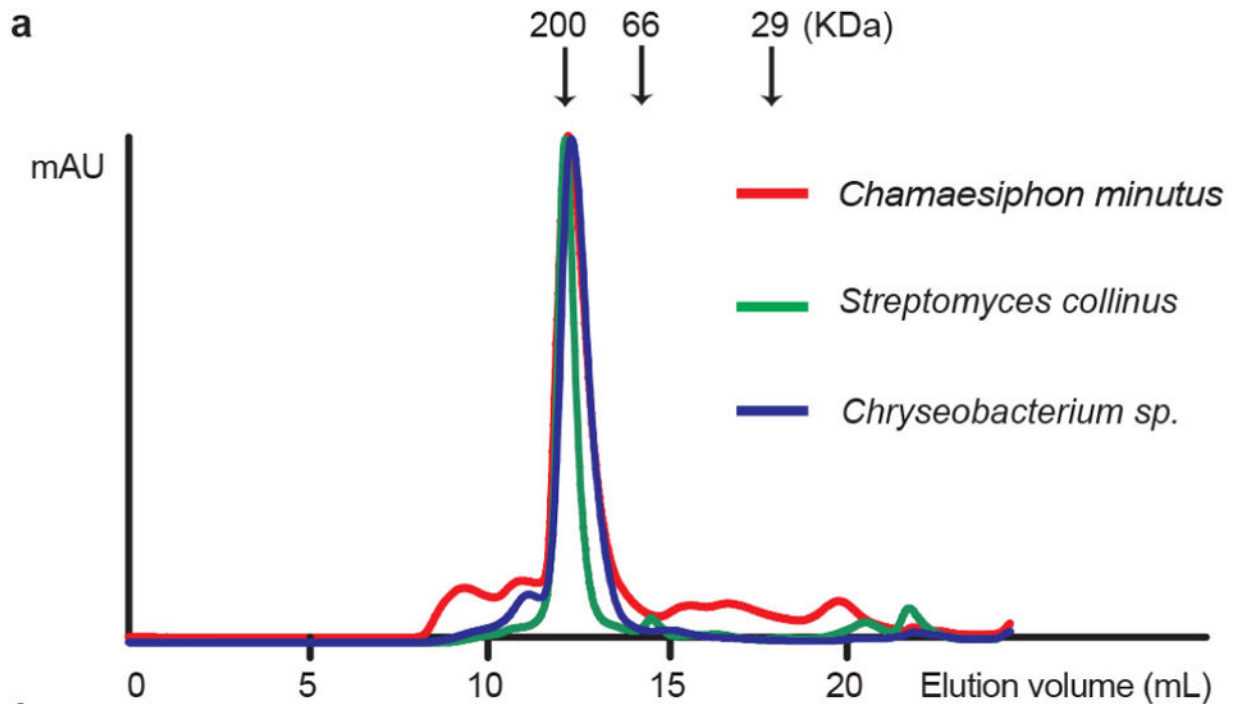
Extended Data Figure 2. Biochemical analysis of bacterial TMEM175s

a, Gel filtration profiles of three purified bacTMEM175s on Superdex-200 (10/30 GL column) in 20 mM HEPES, pH 7.4, 200 mM KCl and 3 mM *n*-decyl-β-D-maltopyranoside. All purified bacTMEM175s eluted as a monodispersed peak at a position much larger than a monomer, indicating oligomerization. Arrows indicate the elution peaks of three standard proteins (29, 66 and 200KDa) on the same column. **b**, Cross-linking reaction of purified bacTMEM175s from *Streptomyces collinus* (left gel) and *Chryseobacterium sp* (right gel) with the cross-linking reagents disuccinimidyl suberate (DSS) and disuccinimidyl glutarate (DSG). Samples are analyzed by SDS-PAGE and detected by coomassie blue staining. The purified protein migrates as multiple bands on SDS-PAGE corresponding to the sizes of monomer to tetramer. Cross-linking reaction promotes the formation of crosslinked tetramer, demonstrating that these bacterial channels form tetramers in solution. For gel source data, see Supplementary Figure 1.

Extended Data Figure 3. Electron density maps of CmTMEM175

a, 2*Fo-Fc* electron density map of one subunit (contoured at 1.5 σ). **b**, 2*Fo-Fc* electron density map of the filter region (contoured at 1.5 σ). The front and back subunits have been removed for clarity. The side chains of the three layers of hydrophobic residues are coloured in magenta.
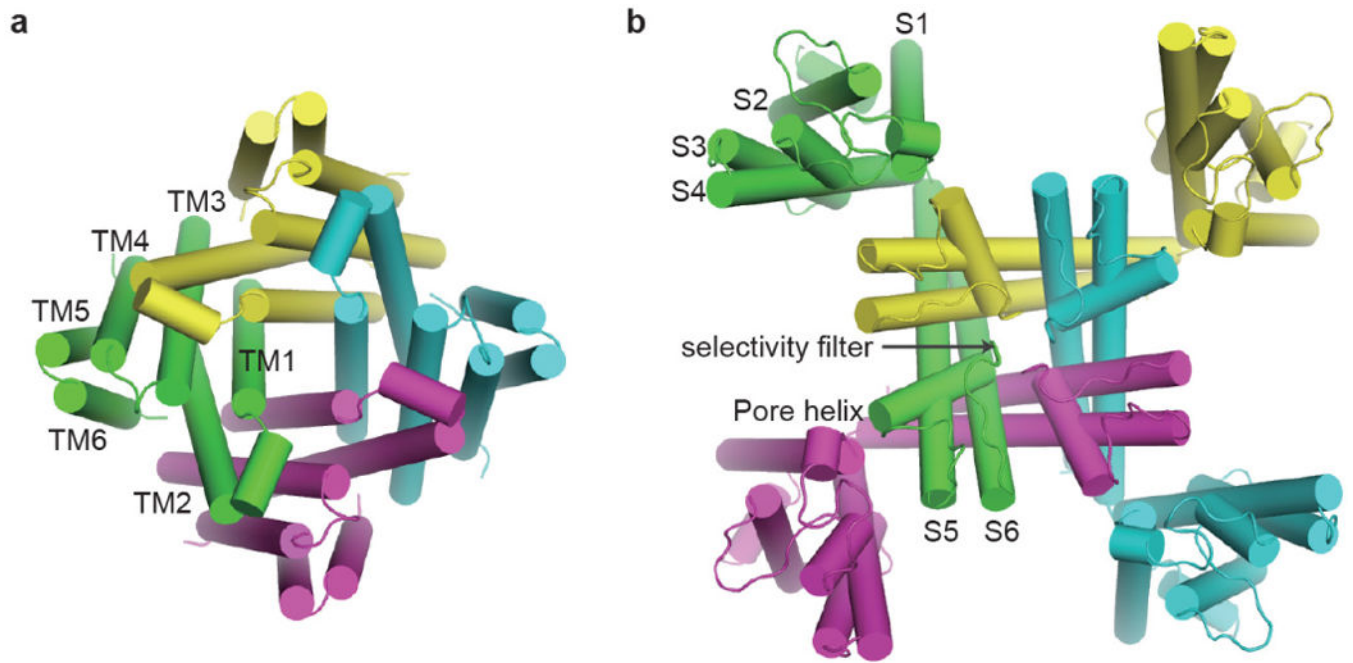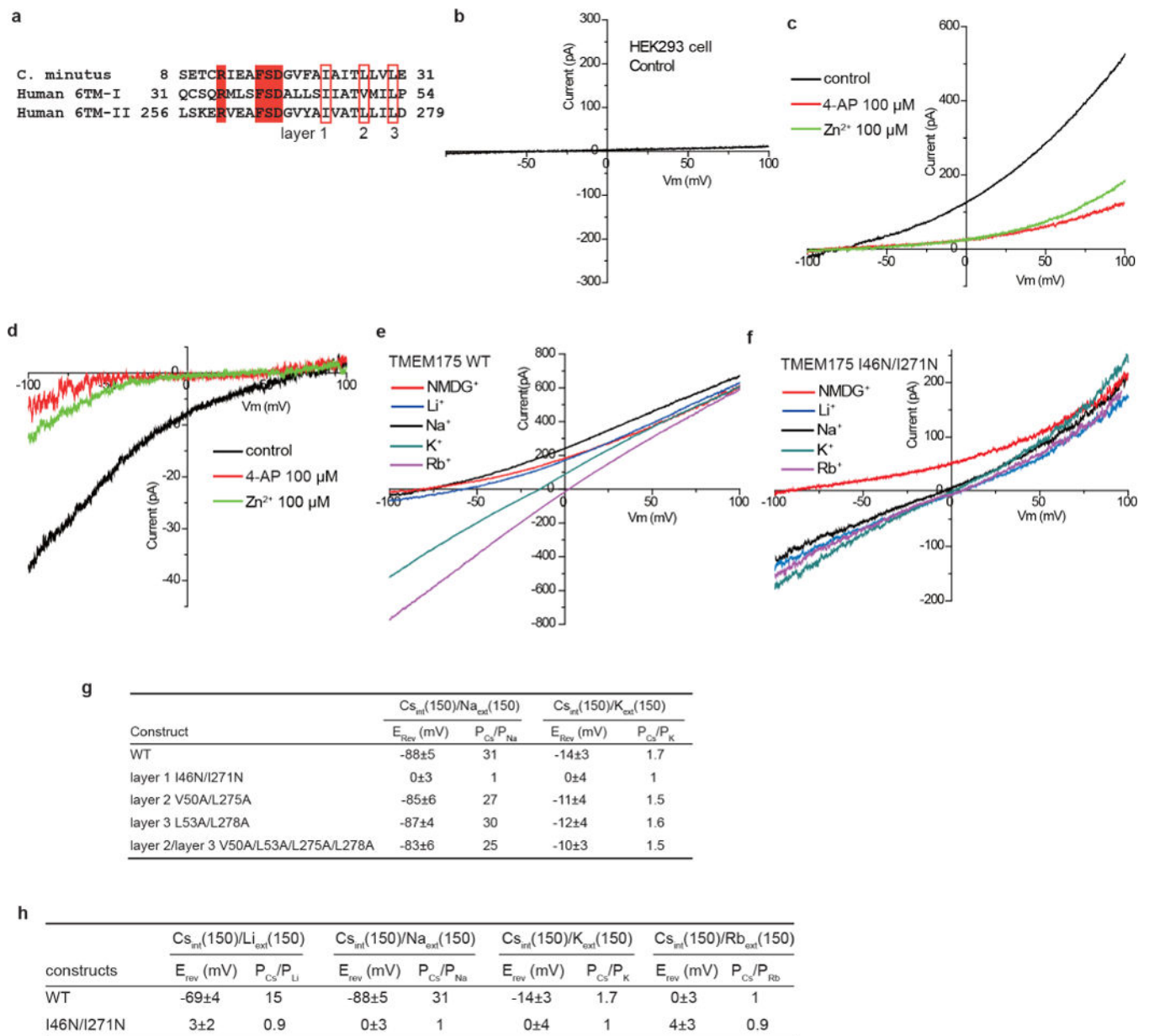
Extended Data Figure 4.
Structural comparison between **a**, CmTMEM175 and **b**, *Shaker*-like K$^+$ channel (Kv1.2-2.1 chimera, PDB code: 2R9R). Each subunit is individually colored. Both structures are viewed from the extracellular side.
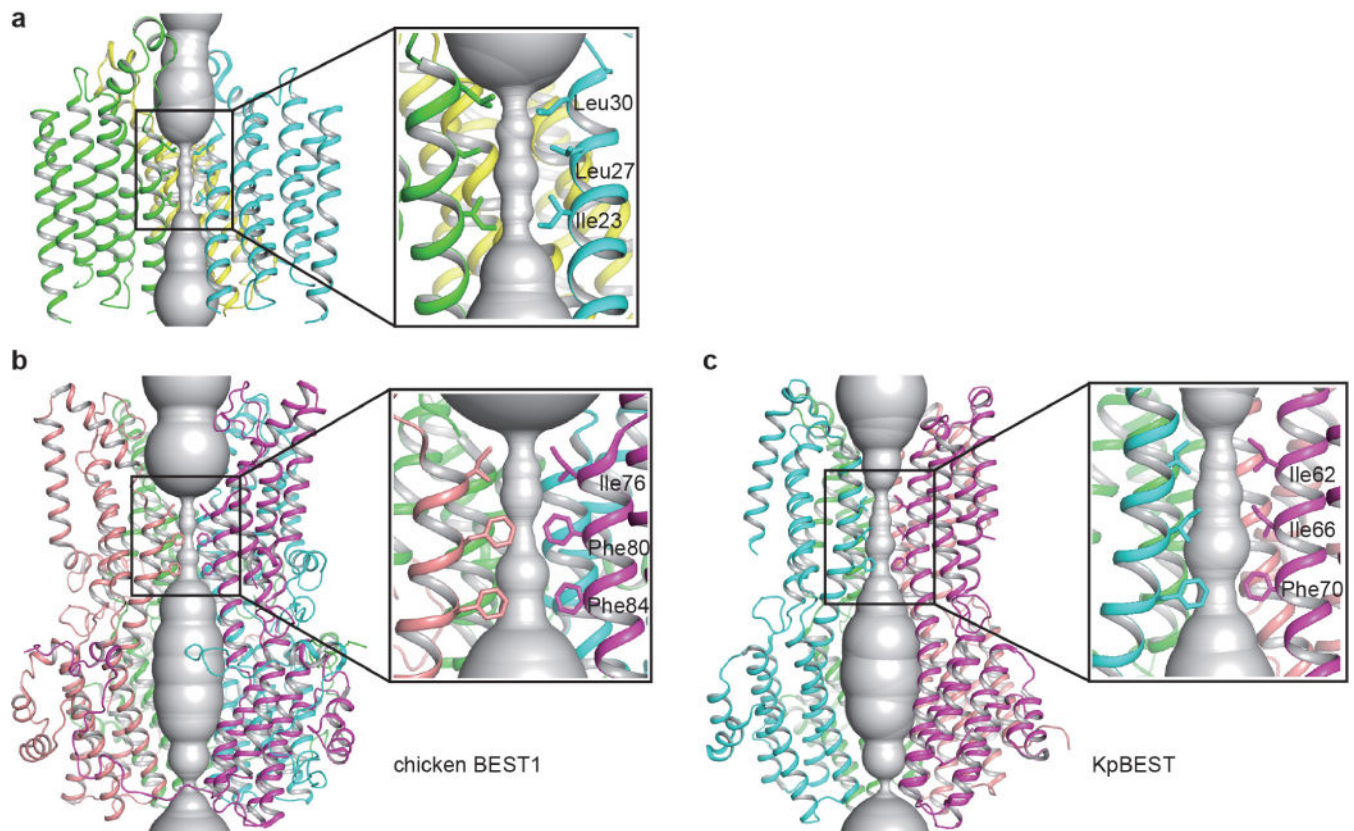
Extended Data Figure 5.
Structural comparison of the ion conduction pathways (shaded grey) from **a**, CmTMEM175, **b**, chicken bestrophin-1 (PDB code: 4RDQ), and **c**, bacterial bestrophin from *Klebsiella pneumoniae* (KpBest, PDB code: 4WD8). Insets show zoomed-in views of the narrow filters.

a, Partial sequence alignment of TM1s from hTMEM175 and CmTMEM175:

```
C. minutus       8 SETCRIEAFSDGVFAIAITLLVLE 31
Human 6TM-I     31 QCSQRMLSFSDALLSIIATVMILP 54
Human 6TM-II   256 LSKERVEAFSDGVYAIVATLLILD 279
                                  layer 1 2 3
```

Extended Data Figure 6. Ion selectivity of human TMEM175 and its pharmacological properties
a, Partial sequence alignment of TM1s from hTMEM175 and CmTMEM175; the three layers of hydrophobic residues are boxed and RxxxFSD motif shaded red. **b**, I-V curve from a control cell. The pipette and bath solutions contain 150 mM Cs^+ and 150 mM Na^+, respectively. **c**, Extracellular Zn^{2+} and 4-aminopyridine (4-AP) block of human TMEM175. Currents were recorded using whole-cell patches with 150 mM of extracellular Na^+ (bath) and 150 mM of intracellular Cs^+ (pipette). **d**, Intracellular Zn^{2+} and 4-AP block of human TMEM175. Currents were recorded using inside-out patches with 150 mM of intracellular Na^+ (bath) and 150 mM of extracellular Cs^+ (pipette). Recordings shown in **c** and **d** indicate that human TMEM175 is sensitive to Zn^{2+} or 4-AP block from both sides. **e**, I-V curves of wild type human TMEM175. Currents were recorded using whole-cell patches in bi-ionic

conditions. The pipette solution contains 150 mM Cs^+ and the bath solution contains 150 mM X^+ (X=NMDG, Li, Na, K, and Rb). **f**, I-V curves of I46N/I271N (at layer 1) double mutant of human TMEM175 in bi-ionic conditions. Currents were recorded using the same conditions as **e**. **g**, Summary of reversal potentials of hTMEM175 and its mutants and the calculated relative permeability between Cs^+ and K^+ or Na^+; shown are mean ± SEM of 5 measurements. **h**, Summary of reversal potentials of human TMEM175 and I46N/I271N mutant with various monovalent cations in the bath solutions and the calculated relative permeability of these ions in comparison to Cs^+.

Extended Data Table 1

Data collection and structure refinement statistics.

Dataset	Native	Hg derivative
Data collection		
Space group	*C2*	*C2*
Cell dimensions		
a, b, c (Å)	152.66, 108.88, 119.33	150.80, 107.85, 118.14
α, β, γ, (°)	90, 117.24, 90	90, 116.72, 90
Wavelength (Å)	1.0332	1.0064
Resolution (Å)	50.00–3.30 (3.36–3.30)[a]	50.00–3.50 (3.36–3.50)
R_{merge}	0.087 (1.596)	0.071 (1.503)
$CC_{1/2}$	(0.581)	(0.633)
I/σ	30.5 (1.4)	26.0 (1.0)
Completeness (%)	99.0 (98.4)	95.5 (95.4)
Redundancy	3.6 (3.4)	7.2 (6.0)
Refinement		
Resolution (Å)	3.7 * 3.6 * 3.3[b]	
No. of reflections	21668	
R_{work}/R_{free}[c]	0.2594/0.2818	
No. atoms		
Protein	5972	
B-factors		
Protein	106.59	
R.m.s deviations		
Bond lengths (Å)	0.011	
Bond angles (°)	1.280	

[a]The number in the parentheses shows the value in the highest resolution shell.

[b]The data was elliptically truncated to $1/3.7$ Å^{-1}, $1/3.6$ Å^{-1} and $1/3.3$ Å^{-1} along a*, b* and c* directions, respectively.

[c]R_{free} was calculated with 5% of reflection data.

Supplementary Material

Refer to Web version on PubMed Central for supplementary material.

Acknowledgments

References

1. Cang C, Aranda K, Seo YJ, Gasnier B, Ren D. TMEM175 Is an Organelle K$^+$ Channel Regulating Lysosomal Function. Cell. 2015; 162:1101–1112. [PubMed: 26317472]

2. Papazian DM, Schwarz TL, Tempel BL, Jan YN, Jan LY. Cloning of genomic and complementary DNA from Shaker, a putative potassium channel gene from Drosophila. Science. 1987; 237:749–753. [PubMed: 2441470]

3. Heginbotham L, Lu Z, Abramson T, MacKinnon R. Mutations in the K+ channel signature sequence. Biophys J. 1994; 66:1061–1067. [PubMed: 8038378]

4. Zhou Y, Morais-Cabral JH, Kaufman A, MacKinnon R. Chemistry of ion coordination and hydration revealed by a K$^+$ channel-Fab complex at 2.0 A resolution. Nature. 2001; 414:43–48. [PubMed: 11689936]

5. Xu H, Ren D. Lysosomal physiology. Annu Rev Physiol. 2015; 77:57–80. [PubMed: 25668017]

6. Luzio JP, Pryor PR, Bright NA. Lysosomes: fusion and function. Nat Rev Mol Cell Biol. 2007; 8:622–632. [PubMed: 17637737]

7. Kolter T, Sandhoff K. Principles of lysosomal membrane digestion: stimulation of sphingolipid degradation by sphingolipid activator proteins and anionic lysosomal lipids. Annu Rev Cell Dev Biol. 2005; 21:81–103. [PubMed: 16212488]

8. Vitner EB, Platt FM, Futerman AH. Common and uncommon pathogenic cascades in lysosomal storage diseases. J Biol Chem. 2010; 285:20423–20427. [PubMed: 20430897]

9. Schulze H, Sandhoff K. Lysosomal lipid storage diseases. Cold Spring Harbor perspectives in biology. 2011; 3

10. Parkinson-Lawrence EJ, et al. Lysosomal storage disease: revealing lysosomal function and physiology. Physiology (Bethesda). 2010; 25:102–115. [PubMed: 20430954]

11. Mindell JA. Lysosomal acidification mechanisms. Annu Rev Physiol. 2012; 74:69–86. [PubMed: 22335796]

12. Xiong J, Zhu MX. Regulation of lysosomal ion homeostasis by channels and transporters. Science China Life sciences. 2016; 59:777–791. [PubMed: 27430889]

13. Jinn S, et al. TMEM175 deficiency impairs lysosomal and mitochondrial function and increases alpha-synuclein aggregation. Proc Natl Acad Sci U S A. 2017; 114:2389–2394. [PubMed: 28193887]

14. Nalls MA, et al. Large-scale meta-analysis of genome-wide association data identifies six new risk loci for Parkinson's disease. Nat Genet. 2014; 46:989–993. [PubMed: 25064009]

15. Heginbotham L, Kolmakova-Partensky L, Miller C. Functional reconstitution of a prokaryotic K$^+$ channel. J Gen Physiol. 1998; 111:741–749. [PubMed: 9607934]

16. Long SB, Campbell EB, Mackinnon R. Crystal structure of a mammalian voltage-dependent Shaker family K$^+$ channel. Science. 2005; 309:897–903. [PubMed: 16002581]

17. Long SB, Tao X, Campbell EB, MacKinnon R. Atomic structure of a voltage-dependent K+ channel in a lipid membrane-like environment. Nature. 2007; 450:376–382. [PubMed: 18004376]

18. Holm L, Rosenstrom P. Dali server: conservation mapping in 3D. Nucleic Acids Res. 2010; 38:W545–549. [PubMed: 20457744]

19. Doyle DA, et al. The structure of the potassium channel: molecular basis of K^+ conduction and selectivity. Science. 1998; 280:69–77. [PubMed: 9525859]

20. Shi N, Ye S, Alam A, Chen L, Jiang Y. Atomic structure of a Na^+- and K^+-conducting channel. Nature. 2006; 440:570–574. [PubMed: 16467789]

21. Aryal P, Sansom MS, Tucker SJ. Hydrophobic gating ion channels. J Mol Biol. 2015; 427:121–130. [PubMed: 25106689]

22. Yang T, et al. Structure and selectivity in bestrophin ion channels. Science. 2014; 346:355–359. [PubMed: 25324390]

23. Kane Dickson V, Pedi L, Long SB. Structure and insights into the function in a Ca^{2+}-activated Cl^- channel. Nature. 2014; 516:213–218. [PubMed: 25337878]

24. Hartzell HC, Qu Z, Yu K, Xiao Q, Chien LT. Molecular physiology of bestrophins: multifunctional membrane proteins linked to best disease and other retinopathies. Physiol Rev. 2008; 88:639–672. [PubMed: 18391176]

25. Vaisey G, Miller AN, Long SB. Distinct regions that control ion selectivity and calcium-dependent activation in the bestrophin ion channel. Proc Natl Acad Sci U S A. 2016; 113:E7399–E7408. [PubMed: 27821745]

26. Li H, Francisco JS, Zeng XC. Unraveling the mechanism of selective ion transport in hydrophobic subnanometer channels. Proc Natl Acad Sci U S A. 2015; 112:10851–10856. [PubMed: 26283377]

27. Zhou X, et al. Self-assembling subnanometer pores with unusual mass-transport properties. Nat Commun. 2012; 3:949. [PubMed: 22805556]

28. Carrillo-Tripp M, Saint-Martin H, Ortega-Blake I. Minimalist molecular model for nanopore selectivity. Physical review letters. 2004; 93:168104. [PubMed: 15525038]

29. Shao Q, et al. Anomalous hydration shell order of Na^+ and K^+ inside carbon nanotubes. Nano Lett. 2009; 9:989–994. [PubMed: 19206198]

30. Otwinowski Z, Minor W. Processing of X-ray Diffraction Data Collected in Oscillation Mode. Methods Enzymol. 1997; 276:307–326. Macromolecular Crystallography, part A.

31. Strong M, et al. Toward the structural genomics of complexes: crystal structure of a PE/PPE protein complex from Mycobacterium tuberculosis. Proc Natl Acad Sci U S A. 2006; 103:8060–8065. [PubMed: 16690741]

32. Schneider TR, Sheldrick GM. Substructure solution with SHELXD. Acta Crystallogr D Biol Crystallogr. 2002; 58:1772–1779. [PubMed: 12351820]

33. Vonrhein C, Blanc E, Roversi P, Bricogne G. Automated structure solution with autoSHARP. Methods Mol Biol. 2007; 364:215–230. [PubMed: 17172768]

34. Abrahams JP, Leslie AGW. Methods used in the structure determination of bovine mitochondrial F1_ATPase. Acta Crystallogr D Biol Crystallogr. 1996; 52:30–42. [PubMed: 15299723]

35. Terwilliger T. SOLVE and RESOLVE: automated structure solution, density modification and model building. Journal of synchrotron radiation. 2004; 11:49–52. [PubMed: 14646132]

36. Emsley P, Lohkamp B, Scott WG, Cowtan K. Features and development of Coot. Acta Crystallogr D Biol Crystallogr. 2010; 66:486–501. [PubMed: 20383002]

37. Adams PD, et al. PHENIX: a comprehensive Python-based system for macromolecular structure solution. Acta Crystallogr D Biol Crystallogr. 2010; 66:213–221. [PubMed: 20124702]

38. Laskowski RA, MacArthur MW, Moss DS, Thornton JM. PROCHECK: a program to check the stereochemical quality of protein structures. J Appl Cryst. 1993; 26:283–291.

39. Smart OS, Goodfellow JM, Wallace BA. The pore dimensions of gramicidin A. Biophysical journal. 1993; 65:2455–2460. [PubMed: 7508762]

40. Baker NA, Sept D, Joseph S, Holst MJ, McCammon JA. Electrostatics of nanosystems: application to microtubules and the ribosome. Proc Natl Acad Sci U S A. 2001; 98:10037–10041. [PubMed: 11517324]

41. The PyMOL Molecular Graphics System, Version 1.7.4. Schrödinger, LLC;

42. Kawate T, Gouaux E. Fluorescence-detection size-exclusion chromatography for precrystallization screening of integral membrane proteins. Structure. 2006; 14:673–681. [PubMed: 16615909]
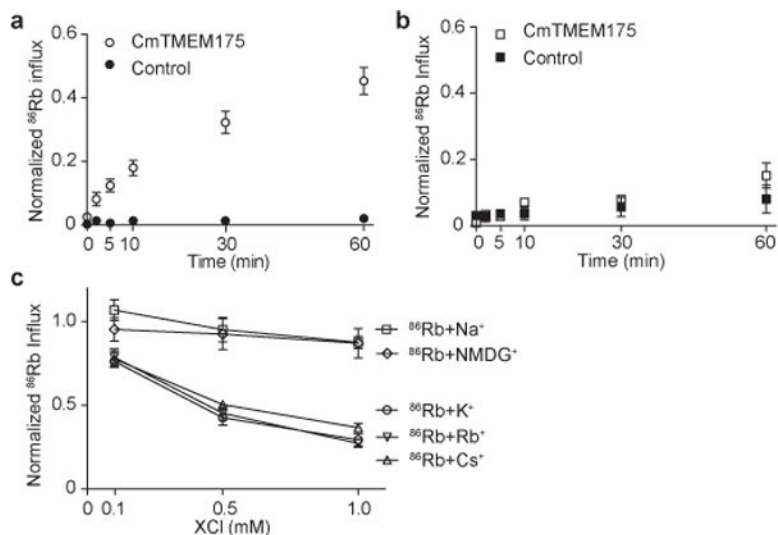
Figure 1.
^{86}Rb flux assay of CmTMEM175. **a**, Time dependent ^{86}Rb influx into CmTMEM175 proteoliposomes prepared in KCl; control liposomes contained no protein. Data are normalized against the maximum ^{86}Rb influx obtained by adding 1 µg/ml of valinomycin to the reaction. **b**, Time dependent ^{86}Rb flux into CmTMEM175 proteoliposomes prepared in NaCl. Data are normalized against the maximum ^{86}Rb influx obtained by adding 10ug/ml of gramicidin A to the reaction. **c**, Competition assay of ^{86}Rb influx in the presence of external monovalent cations. Three concentrations of each cation (0.1, 0.5 and 1.0 mM) were tested. Data are normalized against the control measurement in which no external cations were added. All data points are mean ± SEM of 2-4 measurements.
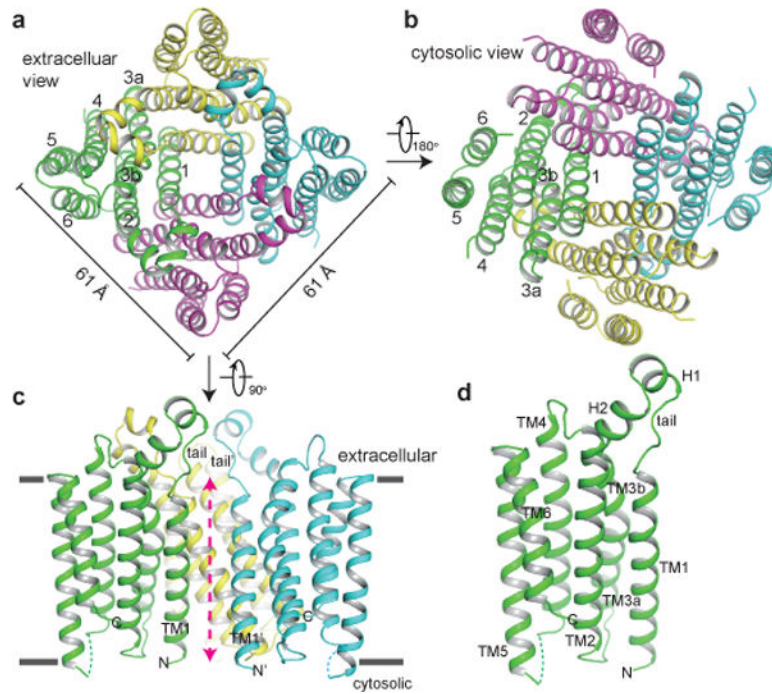
Figure 2.
Overall structure of CmTMEM175. Cartoon representation of the CmTMEM175 tetramer from the extracellular (**a**) and cytosolic (**b**) sides. Each subunit is individually colored. **c**, Side view of CmTMEM175 with the front subunit removed for clarity. Red arrow marks the ion conduction pore axis. **d**, A single subunit of CmTMEM175 in the same orientation as in **c**.
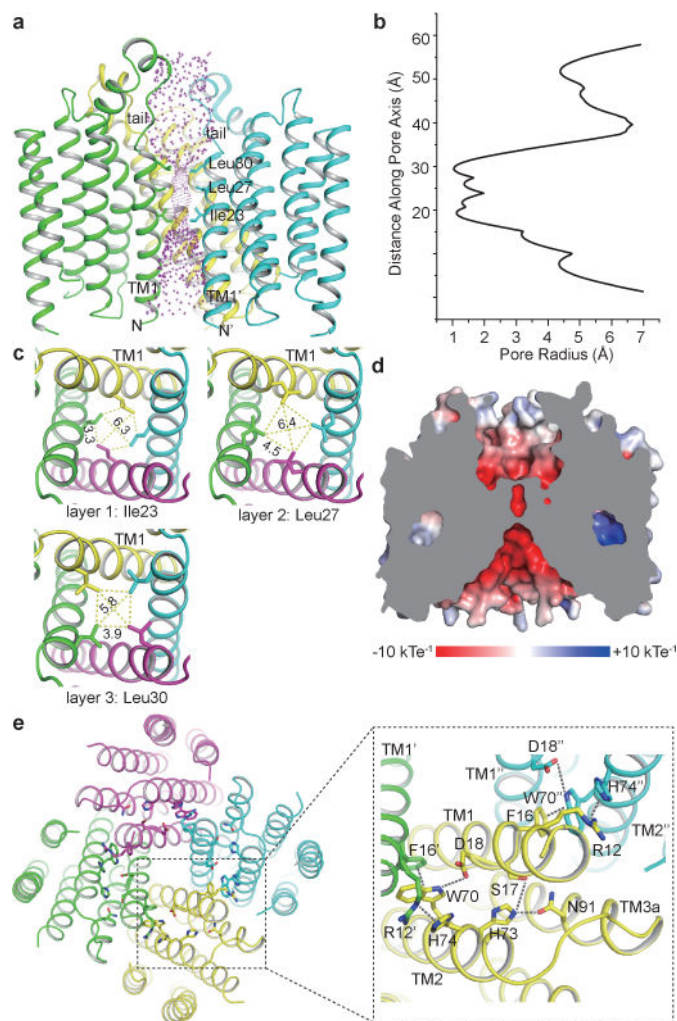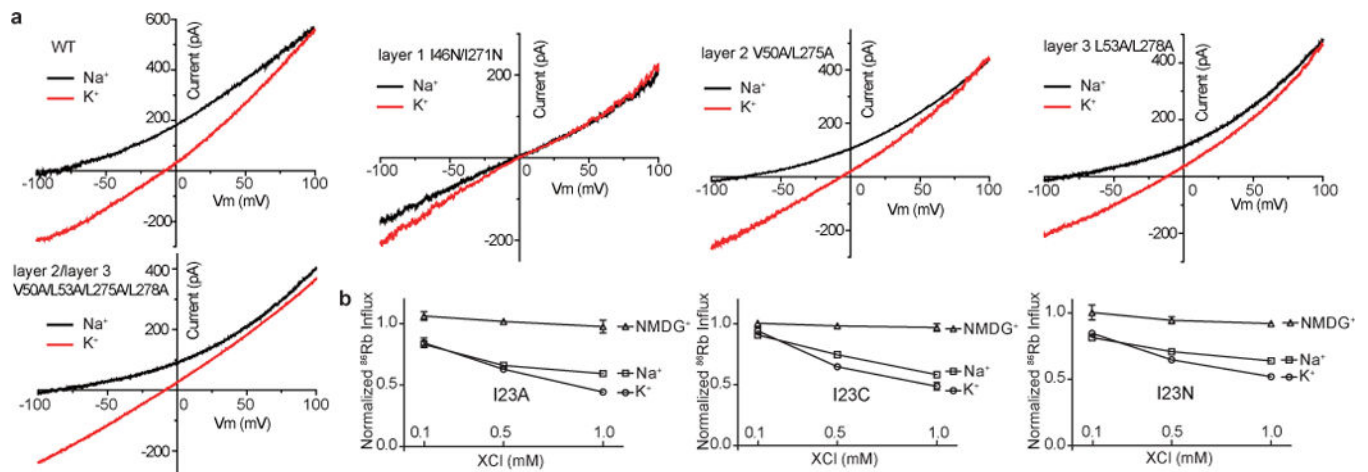
Figure 3.
CmTMEM175 ion conduction pore. **a**, The hour-glass shaped ion conduction pathway shown as purple mesh. **b**, Radius along the central pore axis. **c**, Zoomed-in views of the three layers of hydrophobic residues that form the bottle neck, labeled with atom-to-atom distances in Å. **d**, Cross section through the pore showing the surface electrostatic potential at both entrances. **e**, The RxxxFSD motif in the channel tetramer and zoomed-in view (inset) of the RxxxFSD-mediated inter- and intra-subunit interactions from one subunit (in yellow). Residues from the neighboring subunits are marked with single or double quotation marks.

Figure 4.
Selectivity analysis of hTMEM175 and CmTMEM175. **a**, I-V curves of hTMEM175 and its filter mutations. Currents were recorded using whole-cell configuration, 150 mM Cs$^+$ in pipette and 150 mM K$^+$ (red traces) or Na$^+$ (black traces) in bath. Complete measurement of hTMEM175 selectivity is shown in Extended Data Fig. 6. **b**, ^{86}Rb competition assay on CmTMEM175 Ile23 mutants. Three concentrations of external Na$^+$, K$^+$ or NMDG$^+$ (0.1, 0.5 and 1.0 mM) were tested; shown are mean ± SEM of two measurements.